International Journal of Pharmaceutics 427 (2012) 400–409

Contents lists available at SciVerse ScienceDirect

International Journal of Pharmaceutics

journal homepage: www.elsevier.com/locate/ijpharm

Pharmaceutical Nanotechnology

Chitosan-based luminescent/magnetic hybrid nanogels for insulin delivery, cell imaging, and antidiabetic research of dietary supplements

Jian-Min Shen[a,b], Luan Xu[a], Yan Lu[c], Hui-Ming Cao[c], Zhi-Gang Xu[a], Tong Chen[a], Hai-Xia Zhang[a,*]

[a] Key Laboratory of Nonferrous Metal Chemistry and Resources Utilization of Gansu Province, Lanzhou University, Lanzhou 730000, China
[b] School of Life Sciences, Lanzhou University, Lanzhou 730000, China
[c] School of Pharmacy, Lanzhou University, Lanzhou 730000, China

ARTICLE INFO

Article history:
Received 29 November 2011
Received in revised form 30 January 2012
Accepted 31 January 2012
Available online 7 February 2012

Keywords:
Chitosan
Nanogels
Superparamagnetic iron oxide
CdTe quantum dot (CdTe QD)
Insulin
Antidiabetic effect

ABSTRACT

In this work, the chitosan-based luminescent/magnetic (CLM) nanomaterials were synthesized by direct gelation of chitosan, CdTe and superparamagnetic iron oxide into the hybrid nanogels. The morphology, sizes and properties of the nanogels prepared with different chitosan/QD/MNP ratios and under different processing parameters were researched. Fluorescence microscopy, FTIR spectra and TEM images confirmed the success of the preparation of the CLM hybrid nanogels. Spherical CLM hybrid nanogels with appropriate average sizes (<160 nm) were used for insulin loading. The actual loading amount of insulin was approximately 40.1 mg/g. Human normal hepatocytes L02 cell line was used to explore the effects of additives, such as mangiferin (MF), (−)-epigallocatechin gallate (EGCG), and (−)-epicatechin gallate (ECG) on the insulin-receptor-mediated cellular uptake using insulin-loaded CLM (ICLM) hybrid nanogels. Above 80% of viability of L02 cells were watched at a nanogels concentration of 500 μg/mL whatever the additives existed or not. The study discovered that the fluorescent signals of the ICLM hybrid nanogels in L02 cells were more intense in the presence of MF, EGCG and ECG in medium than in the absence of these components, respectively. These results demonstrate that MF, EGCG and ECG are potentially able to enhance targeting combination of insulin with L02 cells and improve insulin sensitivity in L02 cells. The hybrid nanogels designed as a targeting carrier can potentially offer an approach for integration of insulin delivery, cell imaging, and antidiabetic investigation of dietary supplements.

1. Introduction

Insulin is the top-priority drug of treating Type II diabetes mellitus that involves resistance of glucose and lipid metabolism and inadequate insulin secretion by pancreatic β-cells (Wei et al., 2010; Khan and Mukhtar, 2007). Besides insulin administration, the assistances of dietary components are also regarded as one of the effective approaches to regulate the plasma glucose and cholesterol levels (Yao et al., 2008). Some active components from fruits, such as mangiferin (MF), have received much attention due to their antidiabetic activity (Wilkinson et al., 2008). Several studies have demonstrated that mangiferin or analog was primarily responsible for the inhibition of protein tyrosine phosphatase 1B (PTP1B) (Hu et al., 2007; Klaman et al., 2000) and the regulation of the transactivation of peroxisome proliferator-activated receptor isoforms (PPARs) (Rau et al., 2006) on insulin signaling pathway. In our previous work (Shen et al., 2011), we suggested that mangiferin possessed strong affinity with membrane protein and abundant binding sites on pancreas islet cell membrane and verified that mangiferin could regulate the insulin signaling pathway. Regrettably, the effects of mangiferin on insulin bioavailability are not well understood. In addition, teas are reported to have multiple biochemical and pharmacological activities, such as antioxidant, anticarcinogenic, antiviral and antidiabetic effects (Anrakua et al., 2011; Sandra et al., 2010; Lee et al., 2009). Tea contains many natural polyphenols that are predominately composed of catechins (Hu et al., 2009). Among them, (−)-epigallocatechin gallate (EGCG) and (−)-epicatechin gallate (ECG) are the major active components (Shoji and Nakashima, 2006; Kao et al., 2006) that are confirmed to possess antiobesity and antidiabetic effects (Yang et al., 2001; Marta and Arantxa, 2011; Yun, 2010). However, relative less information is available about the mechanism of EGCG and ECG on antidiabetic effect.

Chitosan, the abundant natural polysaccharide only second to cellulose, has attracted extensive attention because of its versatile properties, such as biological functionality, biocompatibility, nontoxicity, biodegradability (Calero et al., 2010). These attractive properties have provoked the development of chitosan-based particulate systems, especially chitosan nanoparticles which have been adopted as the carriers for delivery of peptides and proteins,

* Corresponding author. Tel.: +86 931 891 2510; fax: +86 931 891 2582.
E-mail address: zhanghx@lzu.edu.cn (H.-X. Zhang).

0378-5173/$ – see front matter © 2012 Elsevier B.V. All rights reserved.
doi:10.1016/j.ijpharm.2012.01.059

antibiotics, antihypertensive drugs, anticancer drugs (Dash et al., 2011; Jia et al., 2009; Trapani et al., 2010). Three major advantages to chitosan particulate systems as drug carriers can be summarized as: protective property, controllable release and high bioavailability. It is crucial for drug carriers to preserve structural integrity and bioactivity of drugs, especially peptides and proteins such as insulin. The encapsulated chitosan nanoparticles can protect insulin from enzymatic degradation and denaturation in the harsh environment in vivo (Trapani et al., 2010), meanwhile can control the release of the encapsulated or adsorbed insulin (Sadeghi et al., 2008). Moreover, chitosan may prolong adhesion time of particles on cell membranes due to its mucoadhesive properties (Sadeghi et al., 2008), which may earn more opportunities for affinity binding between insulin and its receptors on the cell membranes, in turn, improve the bioavailability of insulin (Sinha et al., 2004). Besides that, chitosan also has bioactive properties associated with antidiabetic activity only on its own capacity. It is reported that high molecular weight chitosan demonstrated the potential of reducing hyperglycemia and hypercholesterolemia in streptozotocin-induced diabetic rats (Yao et al., 2008), and the potential of reducing significant levels of cholesterol, in turn, inhibiting the subsequent development of oxidative stress relating to diabetes mellitus in human (Gomes et al., 1995). Chitosan could also improve insulin sensitivity in obese patients and demonstrated a decrease in weight and body mass index (Shukla and Taneja, 2002). Chitosan-based nanoparticles are simultaneously, in short, the very important carriers of insulin delivery and the supplement of antidiabetic drugs. Therefore, it is feasible to develop chitosan nanoparticles as the carrier for exploring effect mechanism of other antidiabetic drugs.

The multifunctional chitosan particulate systems prepared by the incorporation of other function materials, such as magnetic and fluorescent materials, may enlarge its application in biomedicine and biotechnology. Lee et al. developed a chitosan magnetic nanoprobe by the incorporation of superparamagnetic iron oxide into the self-assembled nanoparticles for hepatocyte-targeted magnetic resonance imaging (MRI) (Skrzydlewska et al., 2002). The trans-membrane transport behaviors of chitosan nanoparticles in cells could be detected based on emitting fluorescence signal from fluorescent marker-labeled chitosan (Jia et al., 2009). In fact, chitosan-based magnetic nanocomposites incorporated with fluorescent marker may produce greater potentials compared to chitosan nanoparticles with single property in application for integration of drug delivery, tissue imaging and cell tracking. The superparamagnetic iron oxide in multifunctional nanocomposites can be safely used to label tissues in vivo for MRI tracking (Juang et al., 2010), while fluorescent marker labeled in composites could be tracked to obtain imaging of migration and anchoring of drugs in cells (Cho et al., 2010). Therefore, we can know effect of assistant antidiabetic components through observing comparatively MRI or cell imaging of insulin-loaded multifunctional chitosan particulate systems in tissues or cells in the presence/or absence of these components.

In this paper, to clarify the precise mechanism by which the combination of MF, EGCG and ECG with insulin produced antidiabetic effects, respectively, we synthesized chitosan-coated luminescent/magnetic (CLM) hybrid nanogels by direct gelation of chitosan, CdTe QDs and superparamagnetic iron oxide into the hybrid nanogels and accomplished the subsequent loading of insulin on CLM hybrid nanogels (Scheme 1). After release profiles and cytotoxicity of insulin-loaded CLM (ICLM) hybrid nanogels are evaluated, we explore the effects of above three active components on the insulin-receptor-mediated cellular uptake by human normal hepatocytes L02 cell using ICLM hybrid nanogels.

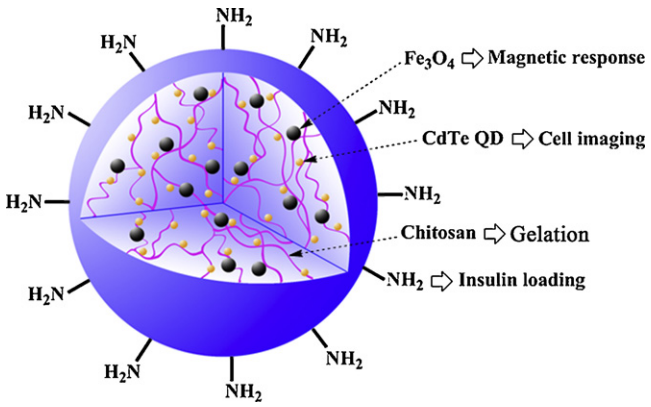

Scheme 1. Schematic diagram of designing multifunctional CLM hybrid nanogel and its potential applications in biomedicine.

2. Materials and methods

2.1. Materials

Ferric trichloride hexahydrate, ferrous chloride tetrahydrate, aqueous ammonia, tellurium powder (purity above 99%), sodium borohydride, cadmium chloride (99%), thioglycolic acid (TGA, 99%), chitosan (80 mesh, MW 22.4 kDa, deacetylation degree above 95%), insulin were purchased from Sigma. RPMI-1640 medium was obtained from Gibco (USA). Calf serum was acquired from Sijiqing Biological Engineering Materials Co., Ltd. (Hangzhou, China). Human normal hepatocytes L02 cell line was obtained from the cell bank of Shanghai Science Academe (China). All other chemicals were of analytical grade. The water used in the study was prepared using a Milli-Q Water Purification System (Milli-Pore, Bedford, MA, USA).

2.2. Synthesis of TGA-capped CdTe quantum dots

The TGA-capped CdTe quantum dots were synthesized by the hydrothermal route combined with previous literature (Guo et al., 2006). Briefly, sodium borohydride and tellurium powder were mixed in 4 mL of deionized water by a molar ratio of 3.4:1 and stirred for 2 h under protection of nitrogen to prepare sodium hydrogen telluride (NaHTe). $CdCl_2$ (1.1 mmol) and TGA (2.0 mmol) were dissolved in 200 mL of water followed by adjustment to pH 8.2. Then, oxygen-free solution containing fresh NaHTe (4 °C) was added to a N_2-saturated $CdCl_2$–TGA solution in an ice-water bath. The concentration ratio of $CdCl_2$, TGA and NaHTe was fixed at 1:2:0.5 for all samples. The mixtures (204 mL) were transferred rapidly into a round bottomed flask with a volume of 500 mL and were vigorously stirred for 1 h in an ice-water bath until faint yellow color. The CdTe precursor solution was maintained at 100 °C in an oil bath and stirred strongly under reflux for 4 h. The flask was cooled to room temperature (about 20 °C). As-prepared product was TGA-capped CdTe nanocrystals with red emission color. According to measurement data of spectrofluorimeter, the PL quantum yield (QY) of the resulting CdTe QDs was determined as 30–40%.

2.3. Synthesis of Fe_3O_4 magnetic nanoparticles (MNPs)

The superparamagnetic Fe_3O_4 nanoparticles were prepared as described (Xu et al., 2006). Typically, ferric trichloride hexahydrate and ferrous chloride tetrahydrate were mixed in 20 mL of deionized water by a molar ratio of 2:1 and stirred and heated to 80 °C until appearance of a dark orange color under protection of nitrogen. Then 12.5 mL of aqueous ammonia was added to above solution,

and the mixture was maintained at 80 °C for 20 min. After cooled to room temperature, the black precipitate was separated with a centrifuge at 6000 rpm for 5 min and washed thoroughly with deionized water and ethanol. Finally, the product was dried in a vacuum oven at 60 °C.

2.4. Synthesis of CLM hybrid nanogels

Firstly, the prepared CdTe nanocrystal was irradiated for 24 h in natural light to obtain high photoluminescence (PL) intensity QDs, and precipitated in excessive anhydrous ethanol, dissolved again in deionized water, and then adjusted pH to 7.5. If not specifically mentioned in the text, CdTe nanocrystal concentrated 10 times was used as the reaction solution. Secondly, the as-prepared Fe_3O_4 MNPs were washed three times with 5% aqueous ammonia by magnetic separation, followed by prepared into suspension (50 mg/mL) with PBS buffer (5 mM, pH 6.0) containing 0.1 M NaCl. Thirdly, at room temperature, the required amount of chitosan powder was added to 2% acetic acid solution and dissolved under sonication for 30 min. The solution was centrifuged at 1000 rpm for 5 min to remove any impurities. Then, the amount of Fe_3O_4 was kept constant at 4 mmol in all cases, while the amount of QDs was varied on the basis of the QD:Fe_3O_4 ratio (1:1, 2:1, 5:1, 10:1, 20:1), the mixture was sonicated for 5 min. The suspension was poured into 24 mL of the required concentration chitosan solution with vigorous stirring, and then was further sonicated for 40 min. Finally, the chitosan-coated QDs/Fe_3O_4 nanoparticles were washed with above PBS to completely remove the excessive unbound precursors in aqueous solution, and followed by freeze drying to obtain dried CLM hybrid nanogels.

2.5. Insulin loading and in vitro release

The synthesized CLM hybrid nanogels were dispersed again in the PBS buffer (5 mM, pH 7.0) containing 0.1 M NaCl by ultrasonication for 30 s to reach a concentration of 10 mg/mL. An estimated amount of insulin was added to CLM hybrid nanogels suspension to prepare an insulin concentration of 2×10^{-5} mol/L. The mixture was shaken gently and incubated for 24 h at 5 °C and then centrifuged at 10,000 rpm for 10 min. The pellets were washed three times with above PBS to completely remove the unbound insulin in aqueous solution, followed by freeze drying to obtain dried insulin-loaded CLM (ICLM) hybrid nanogels. All the supernatants were collected, and the concentration of the unconjugated insulin was assayed using the Bradford method (Bradford, 1976). The amount of loaded insulin on CLM hybrid nanogels was determined according to the changed concentration in solution before and after reaction. All the experiments were carried out in triplicate.

The release profile of insulin in vitro was evaluated in PBS (50 mM, pH = 7.4 and pH 5.3). First, 30 mg of the ICLM hybrid nanogels was soaked in 30 mL of medium at 37 ± 1 °C in a water bath with gentle shaking. 0.5 mL of sample in the solution was withdrawn by means of magnetic separation at defined time periods and analyzed using the Bradford method. An equal volume of fresh medium was added and the amount of insulin released was calculated as described (Fisher et al., 2003). Each experiment was conducted in triplicate and results are presented as mean (standard deviation).

2.6. In Vitro cytotoxicity study

In Vitro cytotoxicity was studied using a MTT method assay. L02 cells (1×10^4 cells/well) were incubated in RPMI-1640 medium containing calf serum (10%) and 1% penicillin–streptomycin in a 96-well plate, in a fully humidified incubator at 37 °C with 5% CO_2. When the cells reached 80% confluence with normal morphology, blank CLM, and ICLM hybrid nanogels with varied concentration were added to cells, respectively, and then these cell dishes were put into incubators at 37 °C for 12 h. In order to evaluate pharmacological effects of MF, EGCG and ECG, in another experiment group, a specified concentration of MF, EGCG and ECG were added to binding medium, while the other conditions were kept constant. The control experiments were also conducted as L02 cells alone in the absence of nanogels and any additive. After incubation for a defined time, the culture medium was removed and 20 μL of MTT reagent (diluted in culture medium, 0.5 mg/mL) was added, followed by incubating for another 2 h. The MTT/medium was removed carefully and DMSO (150 μL) was added to each well for dissolving the formazan crystals. Absorbance of the colored solution was measured at 570 nm using a microplate reader (Bio-Rad, iMark™). All experiments were performed in triplicate.

2.7. Cellular imaging

The cellular images were acquired with a laser confocal scanning microscope (LCSM, ZEISS, LSM 510 Meta, Germany). L02 cells (6×10^4 cells/well) were seeded on a 6-well Plate 37 °C for 24 h. After that, the blank and insulin-loaded CLM hybrid nanogels with a concentration of 100 μg/mL were added to the cell dishes, respectively. After a further 1 h incubation, these nanogel-loaded cells were washed with PBS three times to remove the free nanogels attached on the outer surface of cell membrane and oversize particles adhered to cells. The cellular uptake was detected on LCSM for luminescence imaging under excitation wavelength of 488 nm. The cell imaging of two control experiments were also performed: L02 cells alone, and L02 cells incubated with free additives. All experiments were performed in triplicate.

2.8. Characterization

Fluorescence spectra were recorded on a RF-5310 PC spectrofluorophotometer (Shimadzu, Japan). Transmission electron microscopy (TEM) images were measured with a TecnaiG^2 F30 (FEI, USA) by placing one drop of the samples on copper grids coated with carbon. X-ray energy dispersive (EDX) spectra were obtained on an S-4800 field emission scanning electron microscope with an EDX spectroscopy (Hitachi, Japan). The Fourier transform infrared (FTIR) spectra were acquired with an FTIR spectrometer (NEXUS 670 FT-IR, Nicolet, USA). The magnetic properties were recorded using a vibrating sample magnetometer (VSM) (Lake Shore, USA). The hydrodynamic diameter of the CFLMNPs was determined by dynamic light scattering (DLS) (BI-200SM, Brookharen Instruments Corporation, USA). Others also employed in this work were a high-speed refrigerated centrifuge (Himac, CR 21G, Hitachi, Japan), a sonicator operated at 35 kHz (Elma TI-H-5 MF2, Germany) and level swing bed with temperature controller (Heo Bio-Tech Co., Ltd., Beijing, China).

3. Results and discussion

3.1. Preparation of CLM hybrid nanogels

For the preparation of CLM hybrid nanogels, firstly, the MNPs were treated with 5% aqueous ammonia to obtain MNPs with the sufficient hydroxyl groups on the surface, which can facilitate to bind MNPs to chitosan. And then QDs and MNPs were mixed together using the chitosan as gelation agent according to certain ratios of chitosan/QD/MNP. Fig. 1a–c shows TEM images of the CLM hybrid nanogels prepared by keeping constant the ratio of QDs:MNPs and by varying either the amount of chitosan added or vibrating modes. It is clear that under sonicate mode the QDs

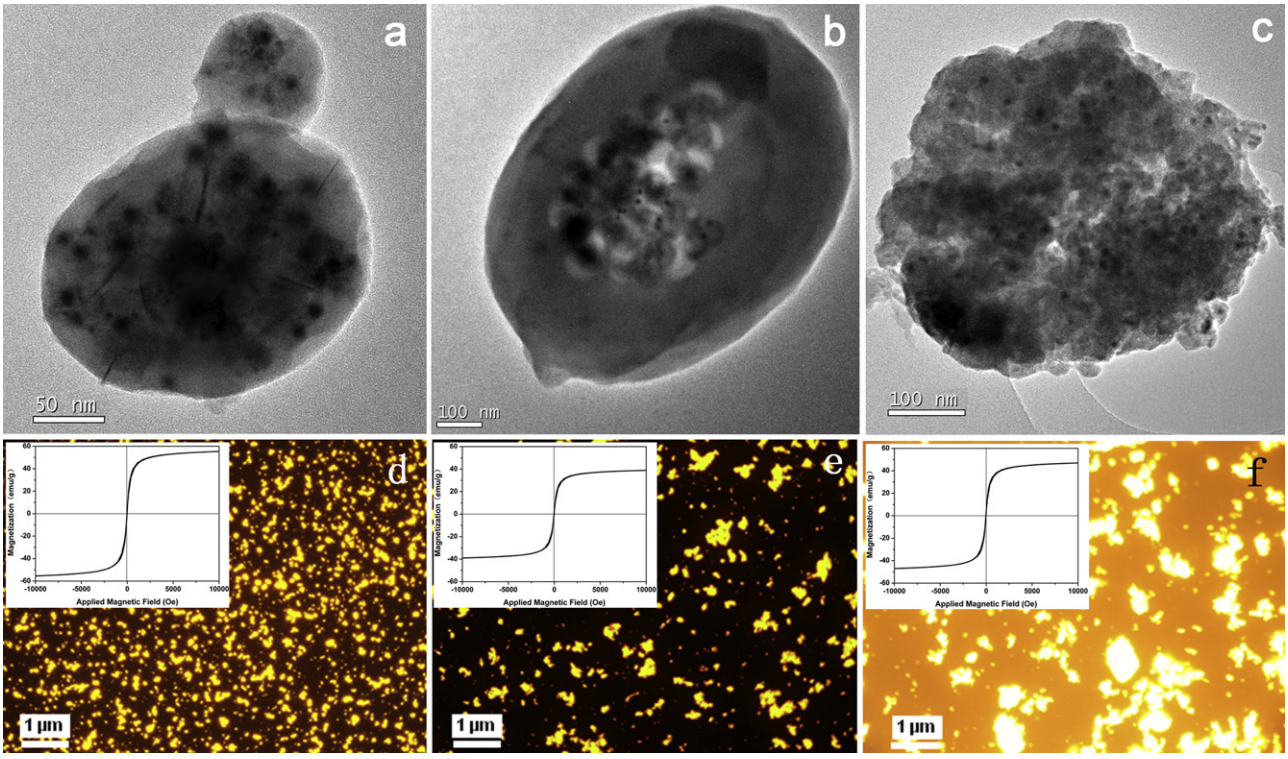

Fig. 1. TEM images (a–c) and corresponding fluorescence microscope images ((d–f) 10×, excitation laser wavelength = 488 nm) and VSM magnetization curves (inset in d–f) of the CLM hybrid nanogels prepared with different ratios of chitosan/QD/MNP ((a) 50/143/57, sonicate binding; (b) 50/143/57, shaking binding; (c) 200/143/57, sonicate binding) at 298 K, respectively. Other conditions: medium pH = 6.0; reaction time = 40 min; and NaCl concentration = 100 mmol/L.

and the MNPs were randomly distributed all over the nanogels (Fig. 1a), and the nanogels tends to small particle sizes, high fluorescence and magnetic properties (Fig. 1d). In the case of vibrating mode, the QDs and the MNPs were squeezed together and clustered round core of the nanogels (Fig. 1b), in addition, the nanogels tends to big particle sizes, relatively weak fluorescence and magnetic properties because of thick chitosan shell (Fig. 1e). When chitosan takes up a high content in ternary precursors, the CLM hybrid nanogels synthesized tends to big sizes and irregular morphology (Fig. 1c), moreover, the nanogels display high fluorescence and moderate magnetism due to the exposure of QDs and MNPs to the surface (Fig. 1f). These results reveal the dependence of the hybrid nanogels properties on feeding ratios of chitosan/QDs/MNPs and vibrating modes in the course of the preparation. In order to obtain the desired nanogels, in this study, we selected the nanogels prepared using ratios of 50/143/57 (chitosan/QD/MNP) and sonicate mode. A typical size distribution from DLS and TEM image containing multiple hybrid nanogels prepared using selected conditions were provided as supporting materials 1 and 2. It can be clearly found that although the suitable feeding ratios of precursors and synthetic conditions can lead to small sized hybrid nanogels (e.g., mean diameter ~160 nm), the mean hydrodynamic diameters from the DLS were larger than these values obtained from TEM image due to dehydration.

The stablity of CdTe QDs and Fe_3O_4 MNPs in the interior of hybrid nanogels was also assessed by examining the fluorescent and magnetic properties of the hybrid nanogels under different conditions (e.g., different pH or temperature). The results showed that the stability of the hybrid nanogels mainly depend on the ratios of chitosan/QD/MNP and vibrating modes in the course of fabrication. On the basis of fluorescence intensity and saturation magnetization measured at pH 5.0–8.0 and at 20–40 °C, CdTe QDs and Fe_3O_4 MNPs in the interior of hybrid nanogels should be stable and be not released. We take into consideration only application in physiology environmental, so the tests under harsh environmental conditions were not done.

Fig. 2 shows the PL intensity of the CLM hybrid nanogels prepared by keeping constant the amount of chitosan and by varying the ratios of QDs:MNPs. The PL intensity from the hybrid bead (at 562 nm) is proportional to the concentration of QDs in the sample. Typically, high QDs:MNPs ratios, i.e., 10:1, corresponding to more amounts of CdTe QDs bound onto the particles, leaded to a strong PL intensity.

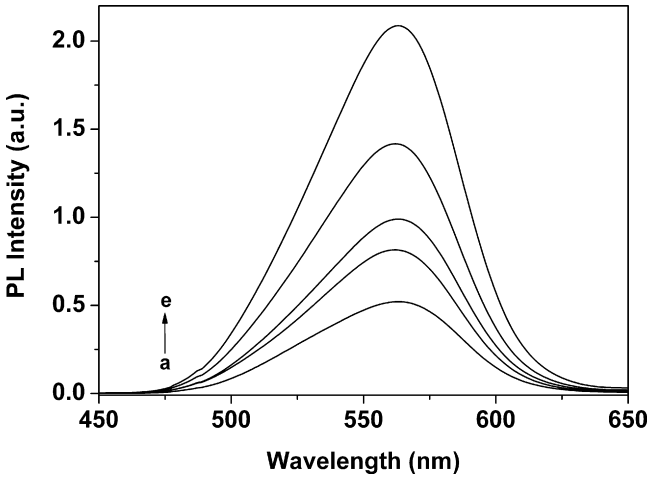

Fig. 2. Dependence of PL on feeding ratios of chitosan/QD/MNP. (a)–(e) Represent PL intensity of as-prepared hybrid nanogels by different chitosan/QD/MNP ratio: (a) 50/100/100; (b) 50/143/57; (c) 50/167/33; (d) 50/182/18; and (e) 50/190/10.

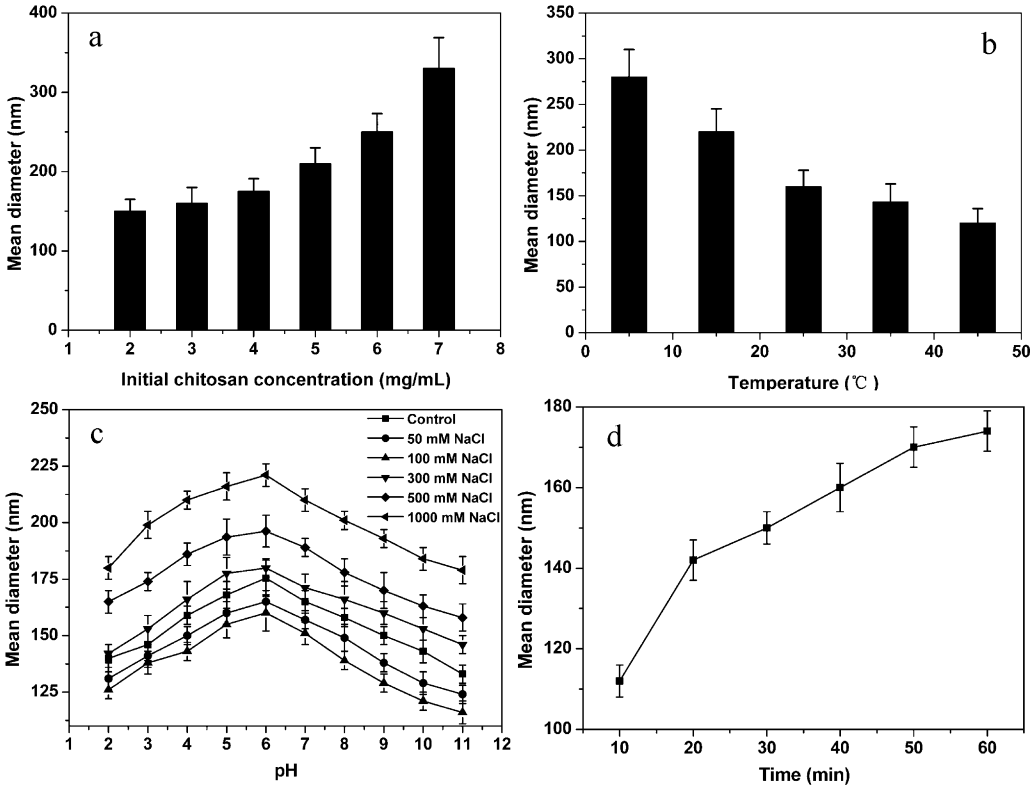

Fig. 3. The average sizes (nm) of the hybrid nanogels prepared at different (a) initial chitosan concentration; (b) temperature; (c) pH combined with NaCl concentration; and (d) reaction time based on DLS measurement. The other constant conditions except a single or two varied parameter: initial chitosan concentration = 2 mg/mL, reaction time = 40 min, pH 6.0, NaCl concentration = 100 mM, temperature = 298 K, Fe_3O_4 = 10 mg/mL, the CdTe:Fe_3O_4 ratio = 2.5:1, sonicating vibration mode.

3.2. Effect of processing parameters on the hybrid nanogels sizes

For in vivo delivery, the particle sizes of 10–200 nm are optimal since they can escape rapid renal clearance (<10 nm) and sequestering by the reticuloendothelial system of the spleen and liver (>200 nm) (Win and Feng, 2005). Thus, the size and stability of drug carriers are important properties that will directly affect the biodistribution and circulation time of the carriers (Schmalenberg et al., 2001). Chitosan molecule is a kind of polyelectrolyte with cation in solution. Chitosan concentration, temperature, pH, salt concentration and reaction time have great influences on chitosan nanogel sizes. Fig. 3 shows the effect of processing parameters on average particle sizes of the hybrid nanogels. As is well seen in Fig. 3a, the average diameter of the resulting hybrid nanogels was about 160 nm when initial chitosan concentration was 2 mg/mL, while the value was more than two times when initial chitosan concentration was 7 mg/mL. At high concentration, each chitosan macromolecule, like irregular mass, twines into the network structure, which leads to the increase of entangling degree and friction force between the molecules, in turn, the viscosity of the solution increases. Thus, the average particle sizes of the hybrid nanogels synthesized are bigger at higher initial chitosan concentration.

It is found that when reaction temperature rises, the resulting hybrid nanogels has a small size (Fig. 3b) because of the increasing mobility, weakened entangling degree and decreasing friction force between the chitosan molecules. However, the rigidity of product synthesized at high temperature is not enough to maintain stable shape due to weak entangling degree, in addition, the PL intensity of the resulting hybrid nanogels will clearly decreased due to change of the surface trap sites of CdTe QDs at high temperature (Biju et al., 2005). In this study, we synthesized the hybrid nanogels at 25 °C to give consideration to two aspects.

It is clear that pH and NaCl concentration also have great effects on sizes of the prepared hybrid nanogels (Fig. 3c) because the pH and ions of the solution can affect the electrical properties of functional groups of chitosan. On one hand, the particle sizes were smaller in an acidic medium than neutral that. The small sizes at pH < 6.0 may be due to electrostatic repulsion of chitosan molecules because of introduction of excessive similar charges in a relatively acid environment. The evident decline of particle sizes at pH > 7.0 is attributed to the poor solubility because of the deformation of chitosan molecules from sphere shape into chain shape. The electrostatic shielding and deformation of chitosan molecules may hinder their entanglement and gelation. On the other hand, the particle sizes were also varied in medium with different NaCl concentration even if pH keeps constant. This is mainly because chitosan molecules bring more ions in a dilute salt solution, which lead to electrostatic repulsion and low viscosity, in turn, aggregation of particles is restrained. The existence of big particles in reaction medium under high NaCl concentration (500–1000 mM) indicated possible aggregation. This could be come down to competition of excess salt with chitosan for water molecules, which resulted in relatively high viscosity and particle aggregation. In this work, we selected the reaction system of pH 6.0 medium containing 100 mM NaCl to obtain the hybrid nanogels with desired sizes (<160 nm). It can be observed in Fig. 3d that the particle sizes of the hybrid nanogels increased gradually with increasing reaction time. In order to control effectively particle sizes, 40 min was considered sufficient to establish equilibrium.

3.3. Characterization of the hybrid nanogels

The success of the preparation of the hybrid nanogels can be verified by comparing the FTIR spectra of products with spectra of various precursors. Fig. 4 shows the FTIR spectra of Fe_3O_4 MNPs,

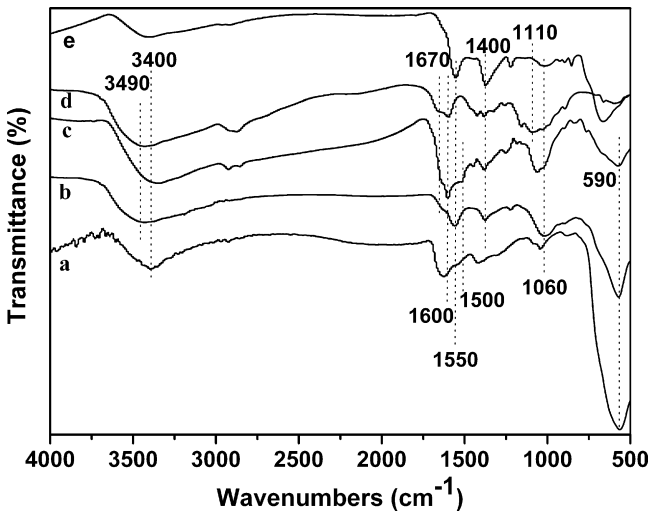

Fig. 4. FTIR spectra of Fe_3O_4 MNPs (a), CLM hybrid nanogels (b), ICLM hybrid nanogels (c), chitosan (d) and CdTe QDs (e).

CdTe QDs, chitosan, CLM and ICLM hybrid nanogels, respectively. As indicated in Fig. 4b, the characteristic peak resulted from the amino group of chitosan occurred at 1600 cm^{-1}, and two main characteristic peaks of TGA-capped CdTe at 1550 cm^{-1} and 1400 cm^{-1} corresponding to the carboxyl antisymmetrical vibration and carboxyl symmetric vibration were observed, respectively. We also find one peak at 590 cm^{-1} (Fig. 4b) related to the Fe—O vibration which did not exist in pure chitosan. These results confirmed that the chitosan-based luminescent/magnetic hybrid nanogels have been achieved.

The nonuniform distribution of QDs and MNPs in a single hybrid nanogel is supported by TEM images and X-ray energy dispersive (EDX) spectra, as shown in Fig. 5. It was seen that the bead shell comprised mainly Fe element (Fig. 5B(a) and C) that contributes to the bead composition (Cu element comes from copper grids), while S, Cd and Te elements were dominating elements in the bead central region (Fig. 5B(b) and D) where the Fe peak, still present, was much less than in shell.

3.4. Insulin loading and pH-regulated release properties in vitro

In order to evaluate the feasibility of the CLM hybrid nanogels as an insulin delivery carrier, we carried out insulin loading studies using CLM hybrid nanogels. Chitosan molecules served as gelation agent possesses a large number of amino groups that some

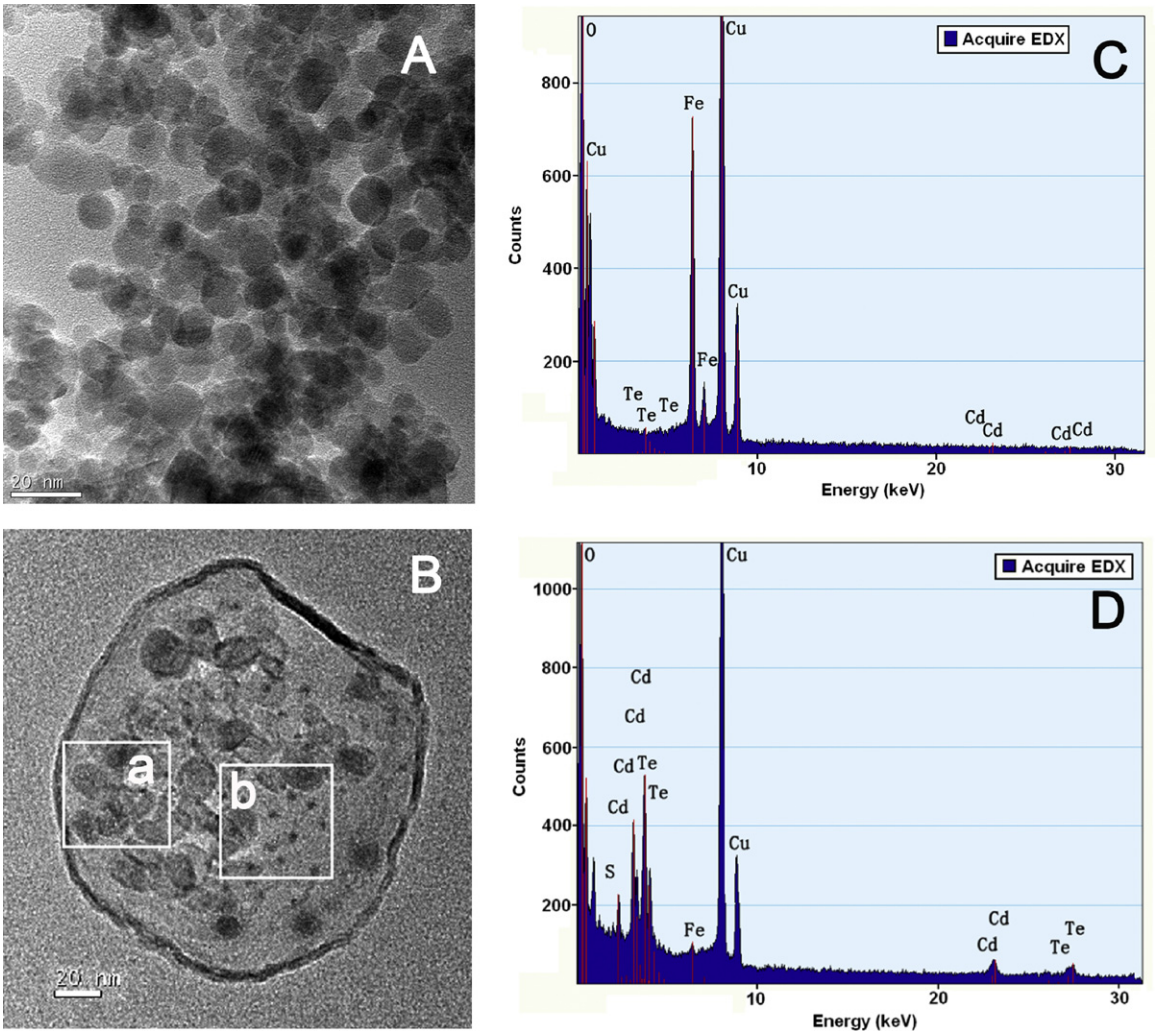

Fig. 5. TEM images of (A) Fe_3O_4 MNPs and (B) a single CLM hybrid nanogel. In (a) and (b) two sections, highlighted in boxes, one on the edge (a) and the other at the center (b) of the nanogel, were selected for the ingredient diagram by EDX as shown in (C) and (D), respectively.

expose to the surface of the hybrid nanogels, which provides the favorable platforms for insulin conjugating via hydrogen bonds, as shown in Scheme 1. In addition, under defined loading conditions (pH 7.0), the insulin molecules carry net negative charges due to acidic isoelectric points of insulin (pI = 5.3). Thus, insulin can be effectively bound to chitosan shell with positive charges by electrostatic attraction. The actual loading amount of insulin on the CLM hybrid nanogels was approximately 40.1 mg/g. Based on FTIR spectrum of the ICLM hybrid nanogels (Fig. 4c), two characteristic peaks resulted from the benzene ring of insulin occurred at 1600 cm^{-1} and 1500 cm^{-1} are observed, confirming the success of the insulin binding.

The release process was examined in a simulated normal body fluid (50 mM PBS, pH 7.4) and an acidic environment (50 mM PBS, pH 5.3) at 37 °C. Fig. 6 shows the release profiles of insulin from the ICLM hybrid nanogels into outer aqueous phase. As shown in Fig. 6, the cumulative release mainly occurred for the first 4 h under two pH systems, and could reach 65% at pH 7.4 and 50% at pH 5.3 within 4 h, respectively. The cumulative release, however, only reached 72% at pH 7.4 and 58% at pH 5.3, respectively, even though the release continued for 8 h. We partly attributed this incomplete insulin release to the moderate hydrophobicity of insulin. The research also indicated that the cumulative release process at pH 7.4 was faster than that at pH 5.3. A major reason is that the solubility of insulin at pH 7.4 is more favorable than at pH 5.3, which leads to optimum release at pH 7.4. By contrast, the release at pH 5.3 is unfavorable because the isoelectric point of insulin is at pH 5.3 where it is unfavorable to dissociate insulin from the ICLM hybrid nanogels. However, we can still observe a considerable amount of the cumulative release at pH 5.3. There are two possible reasons: firstly, the system contains a certain salt that can facilitate the solubility and release of insulin. Secondly, the water content of the chitosan shell was another reason. When at pH 5.3, chitosan molecules are easily soluble to water, so the water content of the shell would be high, and accordingly the permeability of insulin would be higher. When at pH 7.4, the solubility of chitosan molecules are relatively low, so the water content of the shell would be low, and accordingly the permeability of insulin would be

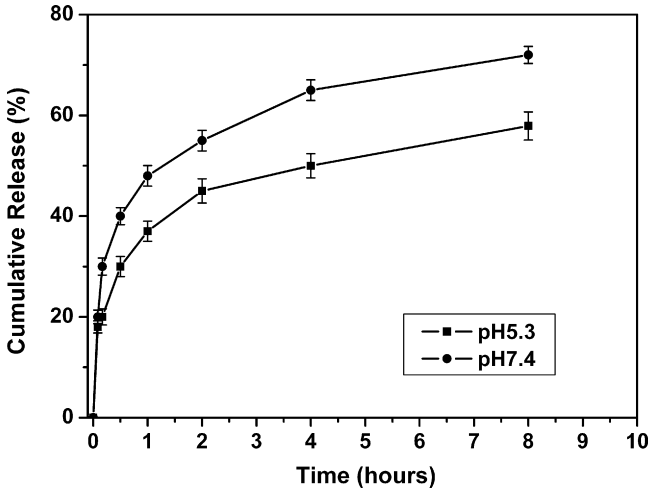

Fig. 6. Release profiles of insulin from the ICLM hybrid nanogels in PBS solutions of pH 5.3 and pH 7.4 at 37 °C.

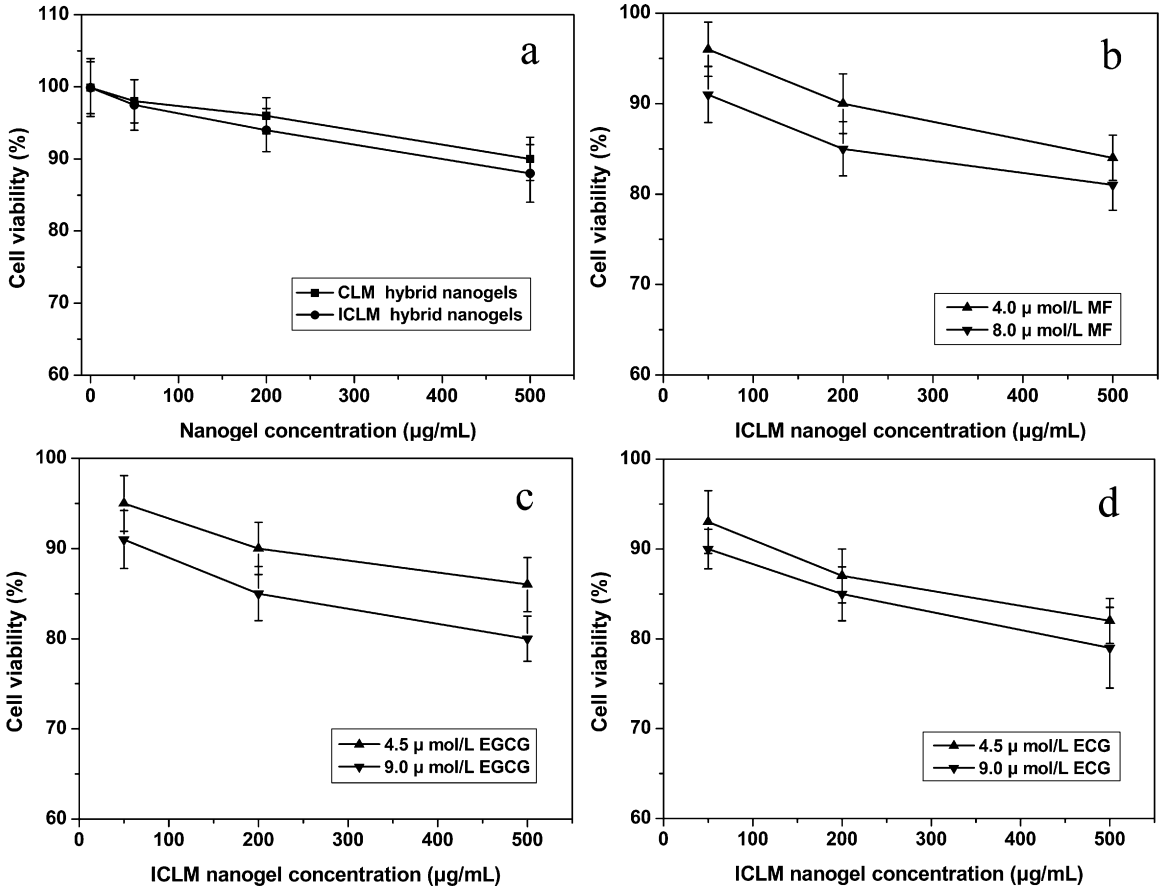

Fig. 7. In vitro cytotoxicity of (a) the CLM and ICLM hybrid nanogels at different concentrations against L02 cells after 1 h incubation. (b)–(d) Show cytotoxicity of ICLM containing MF (4.0 μmol/L and 8.0 μmol/L (b)), EGCG (4.5 and 9 μmol/L (c)) and ECG (4.5 and 9 μmol/L (d)) in medium, respectively.

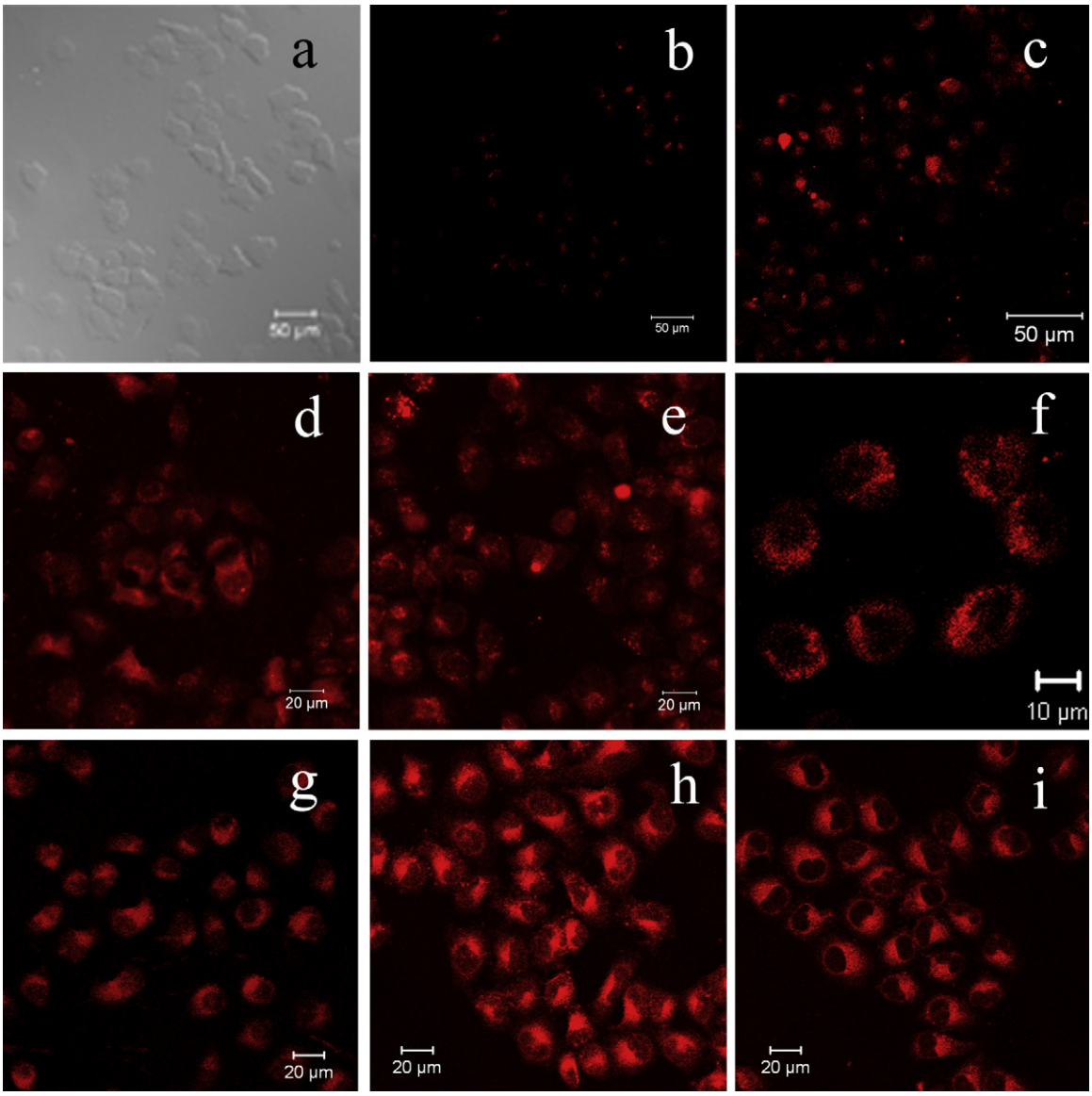

Fig. 8. LCSM images of L02 cells incubated with different materials at 37 °C for 1 h, respectively. (a) Any one of additive MF, EGCG, and ECG with a concentration of 9.0 μmol/L; (b) CLM hybrid nanogels (100 μg/mL); (c) ICLM hybrid nanogels (100 μg/mL). (d)–(i) Show the ICLM hybrid nanogels (100 μg/mL) contain MF ((d) 4.0 μmol/L; (g) 8.0 μmol/L), EGCG ((e) 4.5 μmol/L; (h) 9.0 μmol/L), and ECG ((f) 4.5 μmol/L; (i) 9.0 μmol/L), respectively. Excitation laser wavelength = 488 nm.

lower. Therefore, the comprehensive effect of above various factors resulted in specific release profiles of insulin from the ICLM hybrid nanogels.

In addition, the insulin releasing results clearly demonstrated an initial burst release of insulin. For example, about 20% of insulin could be released at the initial 10 min, while only ~55% (pH 5.3) or ~65% (pH 7.4) of insulin could be released after 8 h. The initial burst release of the insulin may be related with the loading mode of insulin. At first, the added insulin was conjugated chemically to the hybrid nanogel surface to form the first insulin molecule layer through amido bond. Then the excess insulin was adsorbed physically on the first layer insulin thus forming a flabby layer. It is worth noting that although the insulin on the hybrid nanogel surface was unstable, it was not readily removed by motionless washing. In fact, abundant washing have also been performed, but the results after washed more than three times were roughly in accordance with that after washed three times. Therefore, we think that the initial burst release of the insulin should be triggered by shaking in water bath.

3.5. Cytotoxicity studies in vitro

To examine cytotoxicity and cell targeting of the hybrid nanogels, human normal hepatocytes L02 cell line was chosen to incubate with the CLM and ICLM hybrid nanogels in vitro. The control experiment was also performed in the absence of the CLM and ICLM hybrid nanogels. The results showed relatively high cell viability in L02 cell line at different concentration of CLM and ICLM hybrid nanogels (Fig. 7a). 90% and 88% of viability of L02 cells were watched even at a carrier concentration of 500 μg/mL (blank CLM and ICLM hybrid nanogels), respectively, which reveals a low cytotoxicity and favorable cell compatibility for the hybrid nanogels.

We also investigated the cytotoxicity of the combination of the ICLM hybrid nanogels with additive MF, EGCG and ECG by assaying cell viabilities, respectively. The results found that above 80% of cell viabilities were observed at different concentration of the ICLM hybrid nanogels containing any one of three additives in the medium, respectively (Fig. 7b–d), which also reveals a low cytotoxicity and high cell compatibility in the presence of additives.

Three additives, however, have still certain influences on the cell viability.

3.6. Cellular imaging

Fig. 8 shows the typical LCSM images of the L02 cells after being incubated with additive alone, and with the CLM, ICLM hybrid nanogels in the absence/or presence of three additives, respectively. It can be found from the control experiments there was no significant fluorescence from L02 cells treated only with additive MF, EGCG and ECG under similar conditions, respectively (Fig. 8a). The cellular uptakes of the CLM and ICLM hybrid nanogels with a concentration of 100 μg/mL by L02 cells were comparatively analyzed, as shown in Fig. 8b and c. In the case of the ICLM hybrid nanogels, more intense red fluorescence was observed in the cytoplasm (Fig. 8c), indicating that the cellular uptake of the hybrid nanogels can be facilitated by conjugating insulin on their surface. However, there was less fluorescence in the cytoplasm of the cells treated with the blank CLM hybrid nanogels compared to the cells treated with the ICLM hybrid nanogels (Fig. 8b and c). These results clearly demonstrate that the ICLM hybrid nanogels were transported into the L02 cells by an insulin-receptor-mediated endocytosis mechanism, while the blank CLM hybrid nanogels were transported into cells through a non-specific endocytosis process. Besides insulin-receptor mediation, the smart hybrid nanogels should play a critical role in the course of their overcoming cell membrane obstacles to enter the intracellular region.

Fig. 8d–i shows the effects of MF, EGCG and ECG on insulin-receptor-mediated cellular uptake of ICLM hybrid nanogels by L02 cells. Generally speaking, there was more intense fluorescence in the cytoplasm of the cells in the ICLM groups added any one of three additives than in the ICLM-only group, reflecting that MF, EGCG and ECG can increase insulin sensibility, enhance recognition between insulin and its receptor, in turn, improve bioavailability of insulin. This discovery offers the evidence that MF, EGCG and ECG are conducive to the absorption of insulin. As far as the ICLM groups added different additives are concerned, their improving effects have discrepancies. In cells exposed to ICLM hybrid nanogels in the presence of EGCG, the nanogels influx into the cells was significantly more than that in the presence of MF and ECG, in addition, the fluorescence in the cytoplasm had obvious dose effect (Fig. 8e and h), which reveals more remarkable and sensitive improvement effect from EGCG.

4. Conclusions

We have synthesized chitosan-based luminescent/magnetic nanomaterials through direct gelation of chitosan, CdTe QDs and superparamagnetic iron oxide into the hybrid nanogels for integration of insulin delivery, cellular imaging, and antidiabetic investigation of dietary supplements. It was found that the morphologies and properties of the hybrid nanogels depend strongly on feeding ratios of chitosan/QDs/MNPs and vibrating modes. The sizes of the hybrid nanogels were significantly influenced by temperature, pH, NaCl concentration, and reaction time. The hybrid nanogels prepared by optimizing conditions displayed not only sufficient magnetism but also intense fluorescence. The abundant amino groups exposed on the nanogels surface from chitosan provided the favorable platforms for insulin conjugating via hydrogen bonds. The cumulative release of insulin from the ICLM hybrid nanogels mainly occurred for the first 4 h, and showed optimum release at pH 7.4. The cytotoxicity study revealed relatively high cell viability in L02 cell line and favorable cell compatibility at different concentration of CLM and ICLM hybrid nanogels whatever the additives existed or not. The ICLM hybrid nanogels could overcome cell membrane obstacles and were transported successfully into the L02 intracellular region by insulin-receptor-mediated endocytosis. Although the assistant effects of MF, EGCG and ECG had discrepancies, they could enhance sensibility and bioavailability of insulin. It can draw a conclusion that MF, EGCG and ECG are conducive to the absorption of insulin. The multifunctional luminescent/magnetic hybrid nanogels designed as a targeting carrier could potentially provide a way for insulin delivery, cell imaging, and antidiabetic investigation of dietary supplements.

Acknowledgments

This study was supported by the National Natural Science Foundation of China Fund (No. 21105039), and the Fundamental Research Funds for the Central University (No. lzujbky-2012-k09).

Appendix A. Supplementary data

Supplementary data associated with this article can be found, in the online version, at doi:10.1016/j.ijpharm.2012.01.059.

References

Anrakua, M., Fujii, T., Kondo, Y., Kojima, E., Hata, T., Tabuchi, N., Tsuchiya, D., Goromaru, T., Tsutsumi, H., Kadowaki, D., Maruyama, T., Otagiri, M., Tomid, H., 2011. Antioxidant properties of high molecular weight dietary chitosan in vitro and in vivo. Carbohydr. Polym. 83, 501–505.

Biju, V., Makita, Y., Sonoda, A., 2005. Temperature-sensitive photoluminescence of CdSe quantum dot clusters. J. Phys. Chem. B 109, 13899–13905.

Bradford, M.M., 1976. A rapid and sensitive method for the quantitation of microgram quantities of protein utilizing the principle of protein–dye binding. Anal. Biochem. 72, 248–254.

Calero, N., Munoz, J., Ramírez, P., Guerrero, A., 2010. Flow behaviour, linear viscoelasticity and surface properties of chitosan aqueous solutions. Food Hydrocolloid. 24, 659–666.

Cho, H.S., Dong, Z.Y., Pauletti, G.M., Zhang, J.M., Xu, H., Gu, H.C., Wang, L.M., Ewing, R.C., Huth, C., Wang, F., Shi, D.L., 2010. Fluorescent, superparamagnetic nanospheres for drug storage, targeting, and imaging: a multifunctional nanocarrier system for cancer diagnosis and treatment. Nano 4, 5398–5404.

Dash, M., Chiellini, F., Ottenbrite, R.M., Chiellini, E., 2011. Chitosan—a versatile semi-synthetic polymer in biomedical applications. Prog. Polym. Sci. 36, 981–1014.

Fisher, K.A., Huddersman, K.D., Taylor, M., Joan, 2003. Comparison of micro- and mesoporous inorganic materials in the uptake and release of the drug model fluorescein and its analogues. Chem. Eur. J. 9, 5873–5878.

Gomes, A., Vedasiromoni, J.R., Das, M., Sharma, R.M., Ganguly, D.K., 1995. Antihyperglycemic effect of black tea (*Camellia sinensis*) in rat. J. Ethnopharmacol. 45, 223–226.

Guo, J., Yang, W.L., Wang, C.C., He, J., Chen, J.Y., 2006. Poly(N-isopropylacrylamide)-coated luminescent/magnetic silica microspheres: preparation, characterization, and biomedical applications. Chem. Mater. 18, 5554–5562.

Hu, B., Wang, L., Zhou, B., Zhang, X., Sun, Y., Ye, H., Zhao, L.Y., Hu, Q.H., Wang, G.X., Zeng, X.X., 2009. Efficient procedure for isolating methylated catechins from green tea and effective simultaneous analysis of ten catechins, three purine alkaloids, and gallic acid in tea by high-performance liquid chromatography with diode array detection. J. Chromatogr. A 1216, 3223–3231.

Hu, H.G., Wang, M.J., Zhao, Q.J., Liao, H.L., Cai, L.Z., Song, Y., Zhang, J., Yu, S.C., Chen, W.S., Liu, C.M., Wu, Q.Y., 2007. Synthesis of mangiferin derivatives as protein tyrosine phosphatase 1B inhibitors. Chem. Nat. Compd. 43, 663–666.

Jia, X.Y., Chen, X., Xu, Y.L., Han, X.Y., Xu, Z.R., 2009. Tracing transport of chitosan nanoparticles and molecules in Caco-2 cells by fluorescent labeling. Carbohydr. Polym. 78, 323–329.

Juang, J.H., Wang, J.J., Shen, C.R., Kuo, C.H., Chien, Y.W., Kuo, H.Y., Tsai, Z.T., Yen, T.C., 2010. Magnetic resonance imaging of transplanted mouse islets labeled with chitosan-coated superparamagnetic iron oxide nanoparticles. Transplant. Proc. 42, 2104–2108.

Kao, Y.H., Chang, H.H., Lee, M.J., Chen, C.L., 2006. Tea, obesity, and diabetes. Mol. Nutr. Food Res. 50 (2), 188–210.

Khan, N., Mukhtar, H., 2007. Tea polyphenols for health promotion. Life Sci. 81, 519–533.

Klaman, L.D., Boss, O., Peroni, O.D., Kim, J.K., Martino, J.L., Zabolotny, J.M., Moghal, N., Lubkin, M., Kim, Y.B., Sharpe, A.H., Stricker-Krongrad, A., Shulman, G.I., Neel, B.G., Kahn, B.B., 2000. Increased energy expenditure, decreased adiposity, and tissue-specific insulin sensitivity in protein-tyrosine phosphatase 1B-deficient mice. Mol. Cell. Biol. 20, 5479–5489.

Lee, C.M., Jeong, H.J., Kim, S.L., Kim, E.M., Kim, D.W., Lim, S.T., Jang, K.Y., Jeong, Y.Y., Nah, J.W., Sohn, M.H., 2009. SPION-loaded chitosan–linoleic acid nanoparticles to target hepatocytes. Int. J. Pharm. 371, 163–169.

Marta, G.C., Arantxa, R.C., 2011. Dietary phytochemicals and their potential effects on obesity: A review. Pharmacol. Res. 64, 438–455.
Rau, O., Wurglics, M., Paulke, A., Zitzkowski, J., Meindl, N., Bock, A., Dingermann, T., Abdel-Tawab, M., Schubert-Zsilavecz, M., 2006. Carnosic acid and carnosol, phenolic diterpene compounds of the labiate herbs rosemary and sage, are activators of the human peroxisome proliferator-activated receptor gamma. Planta Med. 72, 881–887.
Sadeghi, A.M.M., Dorkoosh, F.A., Avadi, M.R., Saadat, P., Rafiee-Tehrani, M., Junginger, H.E., 2008. Preparation, characterization and antibacterial activities of chitosan, N-trimethyl chitosan (TMC) and N-diethylmethyl chitosan (DEMC) nanoparticles loaded with insulin using both the ionotropic gelation and polyelectrolyte complexation methods. Int. J. Pharm. 355, 299–306.
Sandra, O.H.G., Manuel, G.O., Esperanza, M.A., José, A.R.C., 2010. Chitosan improves insulin sensitivity as determined by the euglycemic-hyperinsulinemic clamp technique in obese subjects. Nutr. Res. 30, 392–395.
Schmalenberg, K.E., Frauchiger, L., Nikkhouy-Albers, L., Uhrich, K.E., 2001. Cytotoxicity of a unimolecular polymeric micelle and its degradation products. Biomacromolecules 2, 851–855.
Shen, J.M., Wang, J., Liu, X.Y., Zhao, C.D., Zhang, H.X., 2011. Study of mangiferin-receptor affinity by cell membrane chromatography using rat pancreas. Med. Chem. Res., doi:10.1007/s00044-011-9697-y, Published online: 22 June 2011.
Shoji, Y., Nakashima, H., 2006. Glucose-lowering effect of powder formulation of African black tea extract in KK-Ay/TaJcl diabetic mouse. Arch. Pharm. Res. 29, 786–794.
Shukla, Y., Taneja, P., 2002. Anticarcinogenic effect of black tea on pulmonary tumors in Swiss albino mice. Cancer Lett. 176, 137–141.
Sinha, V.R., Singla, A.K., Wadhawan, S., Kaushik, R., Kumria, R., Bansal, K., Dhawan, S., 2004. Chitosan microspheres as a potential carrier for drugs. Int. J. Pharm. 274, 1–33.
Skrzydlewska, E., Ostrowska, J., Farbiszewski, R., Michalak, K., 2002. Protective effect of green tea against lipid peroxidation in the rat liver, blood serum and the brain. Phytomedicine 9, 232–238.
Trapani, A., Lopedota, A., Franco, M., Cioffi, N., Ieva, E., Garcia-Fuentes, M., Alonso, M.J., 2010. A comparative study of chitosan and chitosan/cyclodextrin nanoparticles as potential carriers for the oral delivery of small peptides. Eur. J. Pharm. Biopharm. 75, 26–32.
Wei, W., Ma, G.H., Wang, L.Y., Wu, J., Su, Z.G., 2010. Hollow quaternized chitosan microspheres increase the therapeutic effect of orally administered insulin. Acta Biomater. 6, 205–209.
Wilkinson, A.S., Monteith, G.R., Shaw, P.N., Lin, C.N., Gidley, M.J., Thomson, S.J.R., 2008. Effects of the mango components mangiferin and quercetin and the putative mangiferin metabolite norathyriol on the transactivation of peroxisome proliferator-activated receptor isoforms. J. Agric. Food Chem. 56, 3037–3042.
Win, K.Y., Feng, S.S., 2005. Effects of particle size and surface coating on cellular uptake of polymeric nanoparticles for oral delivery of anticancer drugs. Biomaterials 26, 2713–2722.
Xu, X.Q., Deng, C.H., Gao, M.X., Yu, W.J., Yang, P.Y., Zhang, X.G., 2006. Synthesis of magnetic microspheres with immobilized metal ions for enrichment and direct determination of phosphopeptides by matrix-assisted laser desorption ionization mass spectrometry. Adv. Mater. 18, 3289–3293.
Yang, M., Wang, C., Chen, H., 2001. Green, Oolong and black tea extracts modulate lipid metabolism in hyperlipidemia rats fed high-sucrose diet. J. Nutr. Biochem. 12 (1), 14–20.
Yao, H.T., Huang, S.Y., Chiang, M.T., 2008. A comparative study on hypoglycemic and hypocholesterolemic effects of high and low molecular weight chitosan in streptozotocin-induced diabetic rats. Food Chem. Toxicol. 46, 1525–1534.
Yun, J.W., 2010. Possible anti-obesity therapeutics from nature – a review. Phytochemistry 71, 1625–1641.